Collecting more than half the fluorescence photons from a single ion

Robert Maiwald,[1,2,*] Andrea Golla,[1,2,*] Martin Fischer,[1,2] Marianne Bader,[1,2] Simon Heugel,[1,2] Benoît Chalopin,[2,3] Markus Sondermann,[1,2] and Gerd Leuchs[1,2]

[1]*Institute of Optics, Information and Photonics, University of Erlangen-Nuremberg, 91058 Erlangen, Germany*
[2]*Max Planck Institute for the Science of Light, Guenther-Scharowsky-Str. 1/Bldg. 24, 91058 Erlangen, Germany*
[3]*Laboratoire Collisions Agrégats Réactivité, Université Paul Sabatier, 31062 Toulouse Cedex 9, France*

(Received 5 June 2012; published 26 October 2012)

We demonstrate the trapping of a single ion in the focus of a deep parabolic mirror that covers 81% of the solid angle surrounding the ion. Accounting for the reflectivity of the mirror we infer a photon collection efficiency of 54.8% for our setup. The underlying experimentally detected maximum fluorescence rate is 1.91×10^6 s^{-1} from a single ^{174}Yb$^+$ ion, mainly limited by the quantum efficiency of our photon detector. Besides the high collection efficiency, the integration of an ion trap into a parabolic mirror is a key ingredient for efficient coupling of light to a single ion in free space.

DOI: 10.1103/PhysRevA.86.043431 PACS number(s): 32.50.+d, 37.10.Ty, 42.50.Ct

I. INTRODUCTION

Trapped atomic ions are well controllable, pure quantum systems, quite effectively isolated from their environment. Consequently they are the leading system when it comes to demonstrating elementary operations for quantum information processing [1,2] and for highest accuracy optical frequency standards [3]. The fluorescence light emitted by a trapped single ion is the main source of information about both the internal and the external degrees of freedom of this quantum system. For many applications it is thus crucial to be able to detect as much as possible of this light—or as quickly as possible, which is often the same requirement.

In the last few years several groups have worked on increasing the collection efficiency for fluorescence light from a single ion: Following the conventional way of refractive optics based on lenses with high numerical apertures, 4% solid angle coverage per lens have been achieved [4]. Recently this direction has experienced a new impulse by the demonstration of a microfabricated diffractive Fresnel lens with a geometric solid angle of 12% and a measured collection efficiency of 4.2% [5]. Due to electrostatic charging, however, lenses made from dielectric materials cannot be brought arbitrarily close to trapped ions, limiting the achievable numerical aperture. Consequently reflective optics made from metallic surfaces are investigated as an alternative route. Recently an ion trap with a spherical mirror achieved 24% collection efficiency [6].

In this work we follow and expand upon our initial proposal [7,8] of utilizing a parabolic mirror to focus light onto a single atom. Besides being able to cover a much larger solid angle than possible with a single or even a double lens setup, a perfectly shaped parabolic mirror is the optimal focusing element. This leads to an increased field strength at the focus benefiting applications where strong interaction of light and matter is required, for example quantum memories [9] or phase gates [10].

Reversing the light direction in this scenario leads to a system that is equally suitable for efficient fluorescence collection. In the following we will present the experimental realization of such a system.

II. EXPERIMENTAL SETUP

At the heart of our setup lies the combination of a high optical access ion trap with a parabolic mirror. For trapping we use a modified version of the stylus trap demonstrated in Ref. [11]. It consists of a central tubular ground electrode surrounded by a shorter tubular radiofrequency (rf) electrode, both forming a roughly 2-mm-long, tiplike structure capable of trapping ions above it. Four additional electrodes are placed around the tip and are used for micromotion compensation. In contrast to Ref. [11] the ground plane is replaced by a metallic parabolic mirror, providing the necessary outside grounding for the trapping potential [see Fig. 1(a)]. The trap with insulating ceramics, electric connections, a passive low-pass filter-board, and an Yb-filled oven is placed on a linear x-y-z-piezo stage with 250-μm travel in each direction and an active stabilization system based on capacitive sensing with a specified accuracy of 1 nm. The parabolic mirror [12], diamond-turned from a solid block of aluminum (with <4.2% impurities), is separately mounted on a 5-mm linear travel piezo stepper motor that is used for rough alignment along the optical axis. The parabolic mirror has a focal length of $f = 2.1$ mm with a front opening of 20 mm in diameter, resulting in a depth of 11.9 mm. At the vertex the parabolic mirror has three bores: one centered on the symmetry axis with a diameter of 1.5 mm and two 0.5-mm-diameter bores with their central axis pointing at the mirror's focus at an angle of 27° to the optical axis [see Fig. 1(a)]. The central bore is to accommodate the trap electrodes inside the parabolic mirror. The other two bores allow laser beams and a neutral atom beam to enter the mirror.

To load the trap, a Yb-filled steel tube is resistively heated, causing a faint stream of neutral Yb atoms in natural abundance to enter the parabolic mirror through one of the backside holes. In the trapping region this atom stream is met by several superposed laser beams: A laser at a wavelength of 399 nm (≈1 mW, 35-μm beam waist) isotope selectively excites the $^1S_0 \leftrightarrow {}^1P_1$ transition in neutral ^{174}Yb atoms, while another laser at a wavelength of 369 nm (≈300 μW at loading, 20-μm

*These authors contributed equally to this work.

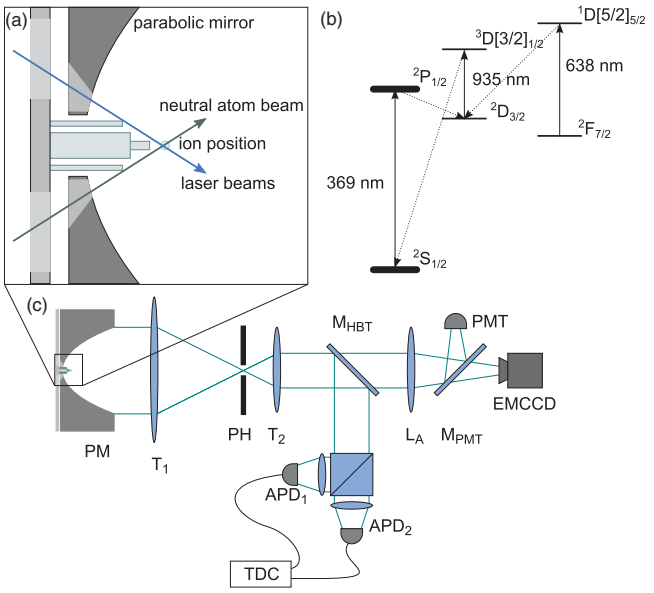

FIG. 1. (Color online) Experimental setup and ion energy levels. (a) Close-up view of the trap geometry, showing the location of a trapped ion in the mirror's focus and the bores in both mirror and trap mounting plate. These bores allow lasers and the neutral atom beam to enter the parabolic mirror from the back. (b) Partial level diagram of $^{174}Yb^+$ (not to scale). (c) Sketch of the detection setup used: A telescope consisting of lenses T_1 and T_2 reduces the size of the beam leaving the parabolic mirror (PM) and is used in combination with a pinhole (PH) for spatial filtering of stray light. The telescope and a lens L_A image either the front plane of the mirror or the ion onto an electron-multipliying CCD camera (EMCCD). Optionally either with mirror M_{PMT} or mirror M_{HBT} the fluorescence light can be directed onto a photomultiplier tube (PMT) or onto a beamsplitter and two avalanche photodiodes (APD_1 and APD_2) connected to a time-to-digital converter (TDC) for a time correlation measurement.

beam waist) ionizes these atoms. The latter laser also provides Doppler cooling on the $^2S_{1/2} \leftrightarrow {}^2P_{1/2}$ transition of the resulting $^{174}Yb^+$ ions [see Fig. 1(b)]. By adjusting the neutral atom flux, this loading process can be optimized to yield a single ion. During loading the Doppler cooling laser is tuned about 40 MHz below the resonance and after loading shifted to the optimum Doppler detuning of $\Gamma/2$, with $\Gamma = 2\pi \times 19.6$ MHz being the natural linewidth of the cooling transition in Yb^+ [13]. For every decay along the cooling transition there is a slight chance of 0.5% for the electron to decay to the metastable $^2D_{3/2}$ level instead [14]; consequently this level is repumped with a laser at a wavelength of 935 nm ($\approx$1 mW, 50-μm beam waist) to the level $^3D[3/2]_{1/2}$ to close the cooling cycle [15]. The Doppler cooling laser and the repumping laser are both frequency stabilized to a temperature-stabilized low thermal expansion cavity in high vacuum. Due to collisions with the remaining background gas, ions are population trapped roughly once per hour in a low-lying, long-lived $^2F_{7/2}$ state [16–18]. To depopulate this level a laser with a wavelength of 638 nm is applied, repumping to the $^1D[5/2]_{5/2}$ state that decays back into the cooling cycle.

The setup described so far resides inside a stainless-steel vacuum chamber with two fused silica windows for laser beams and optical access to the parabolic mirror. The vacuum has a base pressure of about 3×10^{-9} Pa, measured with an ionization pressure gauge.

To provide the necessary rf power to the ion trap it is connected to a helical resonator [19] with a loaded Q factor of 300, that is driven with an input power of 29 dBm at 11.05 MHz from an amplified standard signal generator. The resulting trap frequencies are in the range of 230 kHz for the two nondegenerate radial directions and 480 kHz for the axial direction. The relative positioning of the mirror to the trap determines the exact shape of the trapping potential; consequently the trap frequencies are affected by this positioning. We observe ion lifetimes in excess of 4 h under continuous laser cooling, 935-nm repumping, and occasional repumping with 638-nm light. Without cooling, an ion remains in the trap for a time on the order of 10 min.

The ion's fluorescence from the cooling transition is measured and analyzed in different ways [see Fig. 1(c)]: The parabolic mirror (PM) collimates the light emerging from its focal point into a parallel beam leaving the front aperture. A telescope consisting of lenses T_1 and T_2 with a magnification of 1:2.67 reduces the collimated beam diameter. Additionally a pinhole aperture PH with 300-μm diameter is placed in the focus of this telescope to spatially filter out light not originating from the region around the parabolic mirror's focus. In combination with the telescope a long focal distance lens L_A can be placed to image either the mirror's front opening or the ion onto an electron multiplying charge coupled device (EMCCD) with a pixel size of 16 μm. In the latter case the imaging system has a magnification of 380. Optionally the fluorescence light can be sent onto a photomultiplier tube (PMT) with a removable mirror M_{PMT}, where an additional lens directly in front of the PMT focuses the light onto the detector's active area. We determined the minimal discrimination time of the PMT-based detection to be $\tau = 54$ ns.

Another detection configuration sends the ion's fluorescence with the help of another removable mirror M_{HBT} onto a beamsplitter and two avalanche photodiodes (APDs) to perform Hanbury Brown-Twiss-type experiments [20].

III. RESULTS

When an ion is loaded into the trap and continuously cooled, the resulting fluorescence light emission can be characterized by the intensity distribution of the beam leaving the parabolic mirror. The intensity distribution depends sensitively on the position of the ion relative to the focal point of the parabolic mirror and can be used for alignment. Figure 2(a) shows an image of this intensity distribution taken in the plane of the front aperture of the parabolic mirror when a single ion is located at the mirror's focus. In this case the spatial resolution of the setup allows an ion to be placed at the focus with an accuracy of <1 μm in all three directions. Several features can be observed. The circular front opening of the parabolic mirror is seen, marked in the figure by a segmented circle for better reference. The central bore for the ion trap and the two side holes for lasers and neutral atom beam are visible. Also four thin shadows of compensation electrodes pointing in radial directions are observable near the central hole.

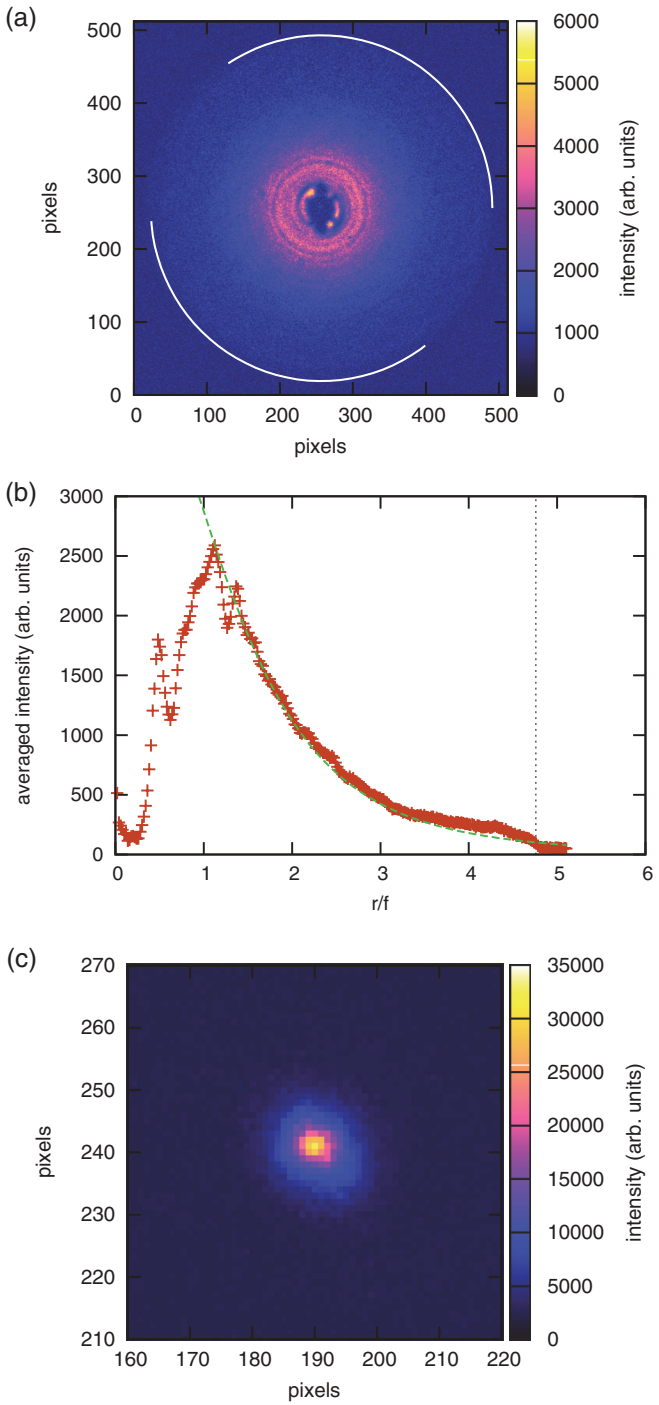

FIG. 2. (Color online) Fluorescence from a single, saturated $^{174}Yb^{+}$ ion located in the focus of the mirror. (a) Background corrected intensity distribution at the mirror's front plane. (b) Intensity distribution of Fig. 2(a) averaged over the azimuth. The vertical dashed line marks the aperture radius of the parabolic mirror. The dashed curve displays the result of a fit with Eq. (1). Data in the interval $r/f = [1.12,4.76]$ have been used for fitting. (c) Focused intensity with a FWHM spot size of 280 nm.

A single, strongly saturated $^{174}Yb^{+}$ ion emits light isotropically and can be considered as an ideal point source. After reflection off the parabolic mirror, the radial intensity distribution of a point source in the mirror's focus ideally reads [21]

$$I(r) = A\left(\frac{r^2}{4f^2}+1\right)^{-2}, \tag{1}$$

with the mirror's focal length f and a scaling factor A. Figure 2(b) shows the radial intensity distribution of Fig. 2(a) averaged over the azimuth, together with a fit to Eq. (1), demonstrating that the light distribution of the ion's fluorescence is indeed in good agreement with a point source after reflection on a parabolic mirror.

When the imaging system is adjusted to focus onto the ion, the spatial resolution can be increased to <250 nm. Figure 2(c) shows the fluorescence of a single ion focused onto the EMCCD with a FWHM spot size of 280 nm, determined from the magnification of our system.

Spurious static electric fields can push the ion from its optimal trapping point and lead to excess micromotion [22]. Ramping up and down the rf power driving the trap by, e.g., 3 dB allows us to iteratively determine the optimal trapping point while adjusting the static voltages on the compensation electrodes and the central electrode of the trap. With this technique and the spatial accuracy of our detection system, we estimate having compensated residual fields to a level of $<7.5\ \frac{\mathrm{V}}{\mathrm{m}}$ in the directions perpendicular to the optical axis. In the direction of the optical axis we complement this technique by the more sensitive time correlation method [22]. The inset in Fig. 3 shows a scan over half the fluorescence line of a Yb^{+} ion after compensation, with a FWHM linewidth of 20.9 MHz, close to the natural linewidth of $\Gamma/2\pi = 19.6$ MHz and slightly power broadened.

By varying the power of the Doppler cooling laser, the saturation of the ion's cooling transition $^2S_{1/2} \leftrightarrow {}^2P_{1/2}$ can be investigated. Figure 3 shows different fluorescence rates over incident laser powers at a constant detuning of $\Delta = \Gamma/2$.

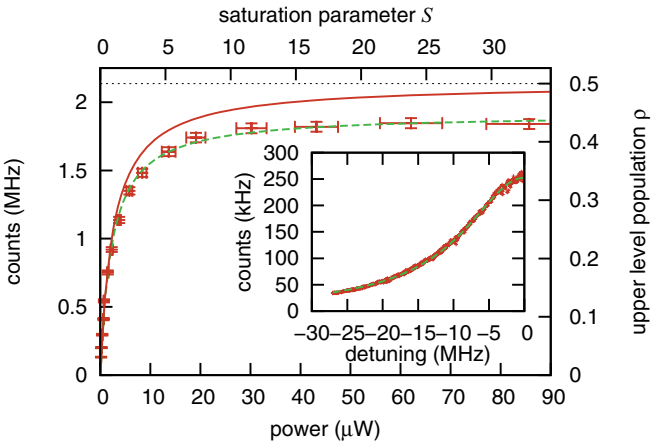

FIG. 3. (Color online) Saturation of the ion's fluorescence for various powers of the cooling laser. The dashed line is a fit of the theoretical saturation curve to the data, and the solid line is the same fit corrected for the finite pulse width of the PMT counts. Inset: Linewidth of the cooling transition $^2S_{1/2} \leftrightarrow {}^2P_{1/2}$ after micromotion compensation and Doppler cooling. The fit (dashed line) to a Lorentzian results in a FWHM of 20.9 MHz. The spectrum is taken at a laser power corresponding to a saturation parameter on resonance of $S_0 \approx 0.14$ and thus consistent with the residual broadening.

The low $^2P_{1/2}$ branching ratio to the $^2D_{3/2}$ level allows us to approximate the cooling transition with a two-level system. With this approximation a certain count rate can be associated with an upper level population $\rho = (S/2)(1+S)^{-1}$ and a laser power with a saturation parameter S, as indicated in Fig. 3. Here the saturation $S = S_0[1 + (2\Delta/\Gamma)^2]^{-1}$ includes the detuning Δ, as opposed to the saturation on resonance S_0. At the highest laser power of Fig. 3, but close to resonance, we measure a maximum count rate of $\nu_m = 1.91 \pm 0.03 \times 10^6\ s^{-1}$ with optimum adjustment. This count rate is corrected by a factor of $1/f_\tau = 1/(1 - \tau\nu_m)$ due to the finite pulse width of the PMT counts. Additionally factoring out the quantum efficiency of the PMT ($\eta_{PMT} = 0.13 \pm 0.02$) and losses in the optical detection system due to the filtering pinhole, nonoptimal lenses, fluorescence filters, and the transmittance of the vacuum window (total transmission of the optical system $T_{OS} = 0.49 \pm 0.05$) we arrive at an inferred collected fluorescence rate of $33.4 \pm 9.6 \times 10^6\ s^{-1}$, i.e., the rate of photons leaving the parabolic mirror. With the solid angle covered by the parabolic mirror ($\eta_\Omega = 0.81$) and its reflectivity ($R_M = 0.67 \pm 0.07$) we infer a fluorescence rate of the ion of $60.9 \pm 23.6 \times 10^6\ s^{-1}$. Neglecting residual ion motion this calculated fluorescence rate can be compared to a theoretical value: At the laser power used the saturation parameter on resonance is $S_0 \approx 66$, which corresponds to a theoretical rate of $\nu_{max} = \Gamma\rho = 60.7 \times 10^6\ s^{-1}$ for an ion at rest. For the finite excitation power used this rate is the upper limit that would be detected under perfect conditions. Considering the high uncertainty of the PMT's quantum efficiency, these values are in excellent agreement.

From the solid angle covered by the parabolic mirror and its measured reflectivity, we deduce that the combined setup of ion trap and parabolic mirror collects 54.8% of the fluorescence emitted by a single ion, and thus surpasses the theoretical limit of a conventional single-sided lens setup with a numerical aperture equal to one. The parabolic mirror trap system thus collects more than every second photon emitted by the ion despite the losses due to the shadowing by the compensation electrodes and the imperfect mirror reflectivity. The complete setup, however, detects 3.14% of the fluorescence photons. The numbers for these considerations are summarized in Table I, together with the absolute maximum fluorescence rate of $\Gamma/2$.

TABLE I. Measured and inferred fluorescence rates and the factors affecting these rates with respect to the detection system and the photon collection system.

Single ion measured rate ν_m	$1.91 \pm 0.03 \times 10^6\ s^{-1}$
Detection system:	
- PMT pulse width correction f_τ	0.90 ± 0.02
- PMT quantum efficiency η_{PMT}	0.13 ± 0.02
- optical system transmission T_{OS}	0.49 ± 0.05
Inferred collected rate ν_c	$33.4 \pm 9.6 \times 10^6\ s^{-1}$
Collection system:	
- parabolic mirror reflectivity R_M	0.67 ± 0.07
- parabolic mirror solid angle η_Ω	0.81
Inferred fluorescence rate ν_{fl}	$60.9 \pm 23.6 \times 10^6\ s^{-1}$
Limit ν_{max} for $S_0 = 66$	$60.7 \times 10^6\ s^{-1}$
Absolute limit $\frac{\Gamma}{2}$ (for $S_0 \to \infty$)	$61.6 \times 10^6\ s^{-1}$

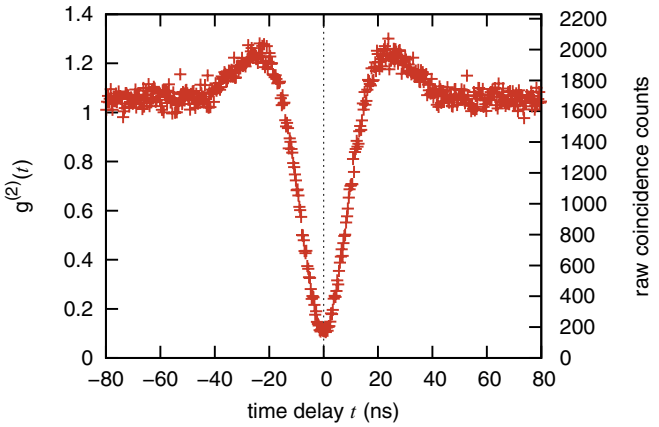

FIG. 4. (Color online) Photon correlation measurement distributing ≈780 000 events from a total acquisition time of 60 s. The histogram is normalized using average count rates and coincidences.

A small portion of the measured light is due to stray light caused by the cooling laser grazing the trap electrodes. This background light is already subtracted in Fig. 3 and is obviously linearly proportional to the power of the cooling laser. As the fluorescence rate saturates with increasing power, there exists a point with maximum signal-to-noise ratio. In our setup this optimal point is at a saturation parameter of $S \approx 0.6$ with a signal-to-noise ratio of about 108.

The single quantum nature of the fluorescent system is verified with a Hanbury Brown-Twiss-type measurement, where the light emitted by the ion is sent onto a beamsplitter with an APD at each output port. The two APDs are connected to a time-to-digital-converter (TDC) that time-tags every photon click detected on one of the APDs. A histogram of the resulting time delays between two photons can be seen in Fig. 4. The rate of photons on each of the APDs is on the order of $300 \times 10^3\ s^{-1}$ with a background below $0.8 \times 10^3\ s^{-1}$. The dip in the correlation histogram at zero time delay with $g^{(2)}(0) < 0.11$ shows the antibunched nature of the emitted photons.

IV. APPLICATIONS

Multiple applications would benefit from a light collection comparable to the one presented in this work. In general, in applications in which the number of emitted photons is used for state detection, the measurement can be sped up considerably. These include optical frequency standards and quantum computation applications. Also, algorithms based on probabilistic measurements of single photons would gain if combined with efficient light collection.

Considering the degree of control one has over single ions, the up-to-months-long trapping times, as well as their robust and reproducible fluorescence rate when comparing to other photon emitting systems such as quantum dots or dye molecules, one could also imagine using a system like the one described here as a luminescence standard. As the fluorescence rate is fixed by the transition's lifetime and as all other limitations are either of geometric nature or material constants, a steady and constant flux of photons can be guaranteed.

Going from light collection to light focusing and thus reversing the light direction, one can take advantage of a

particular convenient feature of our setup: It almost perfectly transforms an incoming radially polarized Laguerre-Gaussian beam into a linear dipole wave traveling towards the focus [7]. With the quantization axis of the ion fixed along the optical axis of the parabolic mirror, the effective solid angle for the focused dipole wave would increase from 81 to 94% for a linear dipole transition in the ion [8,11]. By artificially creating said light field one can increase the light-matter interaction via the strong focusing provided by the mirror.

Two general processes come to mind that can be substantially improved by an efficient light-matter interaction: In the first process single photons are sent into the mirror and due to the strong focusing have a high probability of being absorbed by the ion [7,8,23]. This is a crucial requirement for applications such as quantum memories for the distribution of entanglement in quantum communication networks.

A second process involves a coherent-state pulse that is sent into the mirror to pass the ion and to dispersively interact with it. First results on dispersive interaction in free space have been recently reported in Refs. [24,25]. If the ion is previously prepared in a suitable superposition state, this process will create a coherent cat state and could be used for implementing a phase gate mediated by a coherent light field. Duplicating the setup, one can create an entangled pair of ions in remote traps, constituting a link in a quantum network [26] as proposed in Ref. [27] for cavity-based setups and dispersive interaction.

In view of these exciting applications the successful trapping of single ions inside a parabolic mirror constitutes a major step towards efficient light-matter interaction in free space.

ACKNOWLEDGMENTS

M. S. acknowledges financial support from the Deutsche Forschungsgemeinschaft. G. L. wants to thank the German Federal Ministry of Education and Research for financial support in the framework of the joint research project "QuORep." Fruitful discussions with G. Alber and L. L. Sánchez-Soto are gratefully acknowledged.

[1] J. P. Home, D. Hanneke, J. D. Jost, J. M. Amini, D. Leibfried, and D. J. Wineland, Science **325**, 1227 (2009).
[2] D. Hanneke, J. P. Home, J. D. Jost, J. M. Amini, D. Leibfried, and D. J. Wineland, Nature Physics **6**, 13 (2010).
[3] T. Rosenband *et al.*, Science **319**, 1808 (2008).
[4] S. Gerber, D. Rotter, M. Hennrich, R. Blatt, F. Rohde, C. Schuck, M. Almendros, R. Gehr, F. Dubin, and J. Eschner, New J. Phys. **11**, 013032 (2009).
[5] E. W. Streed, B. G. Norton, A. Jechow, T. J. Weinhold, and D. Kielpinski, Phys. Rev. Lett. **106**, 010502 (2011).
[6] G. Shu, C.-K. Chou, N. Kurz, M. R. Dietrich, and B. B. Blinov, J. Opt. Soc. Am. B **28**, 2865 (2011).
[7] N. Lindlein, R. Maiwald, H. Konermann, M. Sondermann, U. Peschel, and G. Leuchs, Laser Physics **17**, 927 (2007).
[8] M. Sondermann, R. Maiwald, H. Konermann, N. Lindlein, U. Peschel, and G. Leuchs, Appl. Phys. B **89**, 489 (2007).
[9] C. Simon *et al.*, Eur. Phys. J. D **58**, 1 (2010).
[10] Q. A. Turchette, C. J. Hood, W. Lange, H. Mabuchi, and H. J. Kimble, Phys. Rev. Lett. **75**, 4710 (1995).
[11] R. Maiwald, D. Leibfried, J. Britton, J. C. Bergquist, G. Leuchs, and D. J. Wineland, Nature Physics **5**, 551 (2009).
[12] Fabricated at the Fraunhofer Institute for Applied Optics and Precision Engineering in Jena, Germany.
[13] R. W. Berends, E. H. Pinnington, B. Guo, and Q. Ji, J. Phys. B **26**, L701 (1993).
[14] S. Olmschenk, K. C. Younge, D. L. Moehring, D. Matsukevich, P. Maunz, and C. Monroe, Phys. Rev. A **76**, 052314 (2007).
[15] A. S. Bell, P. Gill, H. A. Klein, A. P. Levick, Chr. Tamm, and D. Schnier, Phys. Rev. A **44**, R20 (1991).
[16] H. Lehmitz, J. Hattendorf-Ledwoch, R. Blatt, and H. Harde, Phys. Rev. Lett. **62**, 2108 (1989).
[17] A. Bauch, D. Schnier, and C. Tamm, J. Mod. Opt. **39**, 389 (1992).
[18] M. M. Schauer, J. R. Danielson, A.-T. Nguyen, L.-B. Wang, X. Zhao, and J. R. Torgerson, Phys. Rev. A **79**, 062705 (2009).
[19] W. M. Macalpine and R. O. Schildknecht, Proc. IRE **47**, 2099 (1959).
[20] R. H. Brown and R. Q. Twiss, Nature (London) **177**, 27 (1956).
[21] M. Sondermann, N. Lindlein, and G. Leuchs, arXiv:0811.2098 [physics.optics].
[22] D. J. Berkeland, J. D. Miller, J. C. Bergquist, W. M. Itano, and D. J. Wineland, J. Appl. Phys. **83**, 5025 (1998).
[23] M. Stobińska, G. Alber, and G. Leuchs, Europhys. Lett. **86**, 14007 (2009).
[24] S. A. Aljunid, M. K. Tey, B. Chng, T. Liew, G. Maslennikov, V. Scarani, and C. Kurtsiefer, Phys. Rev. Lett. **103**, 153601 (2009).
[25] M. Pototschnig, Y. Chassagneux, J. Hwang, G. Zumofen, A. Renn, and V. Sandoghdar, Phys. Rev. Lett. **107**, 063001 (2011).
[26] J. I. Cirac, S. J. van Enk, P. Zoller, H. J. Kimble, and H. Mabuchi, Phys. Scr. **1998**, 223 (1998).
[27] P. van Loock, T. D. Ladd, K. Sanaka, F. Yamaguchi, K. Nemoto, W. J. Munro, and Y. Yamamoto, Phys. Rev. Lett. **96**, 240501 (2006).